CMS Physics Analysis Summary

Contact: cms-pag-conveners-exotica@cern.ch 2016/08/05

Search for excited leptons in the $\ell\ell\gamma$ final state at $\sqrt{s} = 13$ TeV

The CMS Collaboration

Abstract

This note presents a search for a possible compositness of electrons and muons using 2.7 fb^{-1} of proton-proton collisions at a centre-of-mass energy of $\sqrt{s} = 13$ TeV collected with the CMS detector in 2015. Excited leptons (ℓ^*) are assumed to be produced via contact interactions in conjunction with the corresponding standard model lepton. The decays considered here are $\ell^* \to \ell\gamma$ with $\ell = e, \mu$. The number of events observed in data is consistent with background processes from the standard model of particle interactions and exclusion limits on the excited lepton mass, and the compositness scale Λ, are set. For the case $M_{\ell^*} = \Lambda$, the existence of excited electrons (muons) up to masses of 2.8 (3.0) TeV is excluded. This analysis sets the most stringent limits on ℓ^* to date.

1 Introduction

The standard model (SM) successfully describes the interactions between particles and agrees with a wealth of experimental results collected during the past 40 years. However, there are still several fundamental questions not explained in the SM. One of them is the mass hierarchy of quarks and leptons. A possible solution is to introduce composite models [1–9] in which quarks and leptons are claimed to be the bound states of three fermions or a fermion-boson pair. These sub-particles are proposed to be bounded by a new strong interaction. If this substructure of fermions really exists, there could be excited states of fermions.

In this analysis we follow the formalism in Ref. [7]. The production of excited fermions via four-fermion contact interaction can be described by an effective Lagrangian:

$$\mathcal{L}_{CI} = \frac{g^{*2}}{2\Lambda^2} j^{\mu} j_{\mu}, \tag{1}$$

where g^{*2} is chosen to be 4π, Λ is the compositness scale, and j^{μ} is the fermion current.

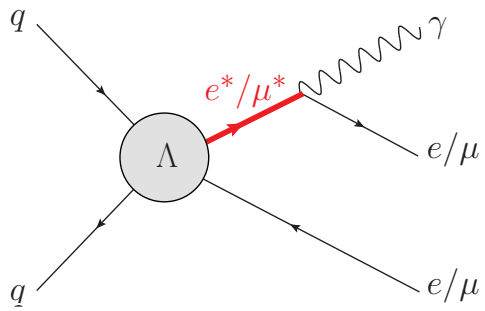

Figure 1: Feynman diagram for the investigated $\ell\ell\gamma$ channels.

This analysis summary presents a search for excited leptons with two same-flavour leptons (e, μ) and one photon in the final state. Figure 1 shows a Feynman diagram of the production of an excited lepton, ℓ^*, via contact interaction and its gauge-mediated decay with emission of a photon.

The analysis strategy follows previous CMS searches for excited leptons as published in Refs. [10, 11]. The latter provides limits on a number of decay channels. The channels with photon radiation, have excluded the existence of excited leptons of mass below 2.5 TeV, under the hypothesis of mass equal to the compositeness scale. Corresponding searches by the ATLAS collaboration [12, 13], not using the full data sample, provide less stringent limits. Searches at LEP [14–17], HERA [18], and the Tevatron [19–22] also have found no evidence for excited leptons.

2 Data and simulated samples

The data for this analysis are collected with the Compact Muon Solenoid (CMS) detector [23] at the CERN LHC with proton-proton collisions at a centre-of-mass energy of 13 TeV in the year 2015. The integrated luminosity corresponds to 2.7 ± 0.1 fb^{-1} [24]. For both channels, eeγ and $\mu\mu\gamma$, data acquisition is triggered by requiring the coincidence of two lepton candidates of the same flavour. In case of the eeγ channel, a trigger with a threshold on the transverse energy of the calorimeter cluster, E_T, of 33 GeV for both electron candidates is used, while the

$\mu\mu\gamma$ analysis relies on a trigger with asymmetric thresholds of 8 GeV and 22 GeV on transverse momentum, p_T, for the two muon candidates.

The ℓ^* signal samples are generated with PYTHIA 8.205 [25, 26] at $\Lambda = 10$ TeV for ℓ^* masses ranging from 250 GeV to 5 TeV in steps of 250 GeV. The production cross section scales with the compositness scale Λ while the kinematics (such as acceptance, decay angle, final state particles and their momenta) and shape of the distributions (such as the final $\ell\gamma$ invariant mass distributions) remain unchanged. The samples are generated with leading order (LO) cross sections. A mass dependent k-factor for next-to-leading order (NLO) QCD corrections is applied, which has been calculated specifically for this analysis at $\sqrt{s}$=13 TeV by the author of Ref. [27]. The resulting higher order corrections range from 1.28 to 1.39.

For the background, we use samples produced with MADGRAPH_aMC@NLO [28], PYTHIA 8.205, and POWHEG [29–31]. For most of the background samples, NLO cross sections are used. The bulk $Z\gamma$ sample is simulated at NLO, while the high-p_T tail ($p_T(\gamma) > 130$ GeV) is only generated at LO. Therefore a k-factor is applied for this high-p_T photon range which has been determined to be a constant 1.37 with a 20% relative uncertainty.

Multiple collisions per beam crossing (pileup) are simulated, and events are weighted to match the vertex multiplicity observed in data.

3 Lepton and photon selection

As illustrated in Fig. 1, the final state contains two same-flavour leptons and a photon. In the very rare cases where more than two lepton or more than one photon candidates are present in the event, the candidates with the largest p_T are selected. A possible signal of excited leptons is expected to appear with a high $\ell\gamma$ invariant mass.

Electrons are reconstructed from clusters of energy deposits in the calorimeters, matched to a track in the tracker. Electron identification exploits the ratio of the energy deposited in the hadron calorimeter to the energy in the electromagnetic calorimeter (H/E), track isolation, isolation in the calorimeter (with $\sim$3% p_T dependence) and proximity to the primary vertex. Selection criteria are optimized for the high-p_T region relevant for this analysis [32, 33]. To be fully above the trigger turn-on an offline threshold of $p_T > 35$ GeV is required. The geometrical acceptance covers the range $|\eta| < 1.44$ and $1.56 < |\eta| < 2.5$. The barrel-endcap interface region between 1.44 and 1.56 is excluded due to its relatively high misreconstruction probability.

The muon candidates have to pass identification criteria that are optimized for the reconstruction of muons with high transverse momentum [33]. Muons with $p_T > 35$ GeV are reconstructed by combining track segments from the inner tracker and at least two muon stations within the geometrical acceptance of $|\eta| < 2.4$. Muons reconstructed with a relative p_T uncertainty above 30% are rejected.

Photons are reconstructed from the energy deposits in the calorimeter, not matched to a track at the collision vertex. In this analysis, the photon candidates are selected in the electromagnetic calorimeter barrel ($|\eta| < 1.44$) and photon identification adopts a multivariate analysis (MVA) technique based on shower shape variables and photon isolation from other particles [34, 35].

In addition, a requirement on the proximity between lepton and photon is applied, $\Delta R = \sqrt{\Delta\eta^2 + \Delta\phi^2} > 0.7$. To maximise the selection efficiency, electron and muon pairs are retained in the analysis without any requirement on their charge.

4 Background determination

Several SM processes contribute to the expected background. All backgrounds arising from two prompt leptons and a prompt photon rely on simulation. The Drell-Yan production is the most important background, mostly originating from associated production with a photon ($Z\gamma$) which has a very similar signature to the signal. This background can be efficiently rejected by the 'Z-veto selection': pairs formed by two same-flavour leptons are required to have an invariant mass above 116 GeV. After this selection criterion is applied, $Z\gamma$ events amount to nearly two-thirds of the total expected background. The $Z\gamma$ background simulation was done at NLO for photons with p_T <130 GeV. For those events, which are simulated at LO, higher order corrections are calculated.

The contribution of diboson events (labelled VV in the plots) is small. Only events with an additional high energy photon or those where an electron is misidentified as a photon contribute. These background contributions were simulated using PYTHIA. Events where an additional prompt photon is produced together with a top pair ($t\bar{t} + \gamma$) are simulated with MADGRAPH, normalized to the next-to-next-to-leading order (NNLO).

An uncertainty of 10% on the cross section of the dominant $Z\gamma$ background is assumed, taken from our studies at $\sqrt{s}$=8 TeV. It is the dominant systematic uncertainty which impacts the total background at a net level of 7% given that 2/3 of the background arises from $Z\gamma$. On the k-factor for the very few $Z\gamma$ events with photon p_T >130 GeV a constant 20% is applied. The second most important uncertainty in both channels, is due to the MC statistics.

Further contributions are due to events with two genuine leptons and a jet which has been misidentified as a photon. This background has been estimated from data using events in a control region defined by photon candidates failing the photon selection and all other signal kinematic selections applied. The number of events in this control region scaled by a 'fake ratio' gives the estimate of this background. The 'fake ratio' is defined as a ratio of misidentified photon candidates expected to pass the selection criteria to that of all photon candidates failing this selection. This ratio is measured in bins of photon p_T by fitting template distributions of MVA variable for photons and background events to the data sample selected for this analysis before the application of the Z-veto selection. For photons, a template distribution of MVA variable is obtained from simulated $W\gamma$ samples where the photon candidates are matched to a photon at generator level. A template distribution for misidentified photons is obtained from dilepton data. The binning in p_T is driven by the statistical uncertainty and ranges from 35 GeV to 120 GeV. The fake ratio is about 0.1 and nearly p_T independent. When applying the fake ratio to data, it results in about 5-15% of the total background being due to jets faking a photon. The fake ratio has been determined separately in the electron and muon channel, yielding very similar results. Overall, the estimates of fake photon contribution using this method are in good agreement with simulation.

In the electron channel jets or photons faking an electron also play a role, unlike the muon channel. The largest contributions come from processes such as $W(\rightarrow e\nu)$ + jet + γ where the jet in the event is misidentified as an electron. The misidentification rate is calculated as the ratio between the number of candidates passing the electron selection criteria with respect to those satisfying looser selection criteria. This ratio is estimated as a function of p_T in bins of η using a data sample selected with single-photon triggers [33]. The jet to electron misidentified background in e^* is estimated by applying this misidentification rate to a sample passing all selection requirements, except requiring one of the electron candidates to fail the electron identification criteria and pass instead the loose identification requirements. The systematic uncertainty on the estimate of misidentified electrons is determined using a sample of events

containing two reconstructed electrons.

5 Analysis strategy and selection steps

The following analysis steps should discriminate a potential signal from the SM background:

1. Following the application of triggers, lepton and photon objects are selected as described in Section 3.
2. To suppress the primary Drell-Yan background, events with selected lepton pairs with invariant mass below 116 GeV are rejected.
3. Two $\ell\gamma$ invariant masses are computed, denoted $M_{\ell\gamma}^{\text{min}}$ and $M_{\ell\gamma}^{\text{max}}$ in increasing order of mass. For the final result a search window in the shape of an inverted L in $M_{\ell\gamma}^{\text{min}}$, $M_{\ell\gamma}^{\text{max}}$ space selects the signal region as a function of M_{ℓ}^{*}.

5.1 Data and backgrounds after event selection

The remaining number of events for the various background contributions after application of the signal selection and Z veto are shown in Table 1. The expected backgrounds are determined as described in Section 4.

Table 1: Number of observed events in data compared to expected backgrounds with uncertainties after all selection steps except the L-shaped search window.

	Electron channel	Muon channel
$Z\gamma \to \ell\ell\gamma$	$28.5 \pm 2.3 \pm 6.7$	$28.2 \pm 1.7 \pm 2.8$
$t\bar{t}\gamma$	$1.4 \pm 0.1 \pm 0.2$	$2.0 \pm 0.1 \pm 0.2$
VV	$2.5 \pm 0.6 \pm 0.7$	$0.33 \pm 0.21 \pm 0.02$
Misidentified Photons	$2.1 \pm 0.5 \pm 0.8$	$5.1 \pm 0.7 \pm 2.8$
Misidentified Electrons	$1.8 \pm 0.3 \pm 0.9$	–
Sum background	$36.3 \pm 2.4 \pm 6.9$	$35.7 \pm 1.9 \pm 4.0$
Data	44	41

5.2 Invariant masses $M_{\ell\gamma}^{\text{min}}$ and $M_{\ell\gamma}^{\text{max}}$

There are two possibilities to reconstruct the mass of a hypothetical excited lepton: with the lepton coming from the decay of the excited lepton or with the lepton that was produced in association with the excited lepton. From the final state, both possibilities are indistinguishable. Thus, both possible invariant masses are calculated and in the following referred to as $M_{\ell\gamma}^{\text{min}}$ and $M_{\ell\gamma}^{\text{max}}$ in increasing order of mass. The corresponding distributions are shown in Fig. 2.

Plotting $M_{\ell\gamma}^{\text{min}}$ versus $M_{\ell\gamma}^{\text{max}}$ in a 2D plane leads to a distribution where the expected background tends to be at low invariant masses, while a potential signal has the form of an inverted "L" around the excited lepton mass as shown in Fig. 3. This feature of the signal distribution is used to define an L-shape search region used in this analysis.

This final selection results in a search region that is defined in the two dimensional distributions of $M_{\ell\gamma}^{\text{min}}$ and $M_{\ell\gamma}^{\text{max}}$. Contributions from data, background, and signal are evaluated for each simulated ℓ^* mass in a sliding search window. At low masses, these search windows are narrow

and consist of a common lower and an upper threshold for either quantity, $M_{\ell\gamma}^{\min}$ and $M_{\ell\gamma}^{\max}$. For example, for μ^* = 250 GeV, the search window is between 241 - 259 GeV. In the electron channel one has to consider the impact of the correlated electron and photon uncertainties (see Table 2) on the signal acceptance. If one considers a narrow window similar to μ^* at low mass points, one can have $\sim$50% impact on the signal acceptance due to energy scale and resoltion. To avoid such a large systematics on the signal efficiency due to energy scale and resolution the e* windows are increased to cover $\pm$10% around the simulated e* mass; for the example of e* = 250 GeV the search window is 225 - 275 GeV. For masses of $M_\ell^* \geq$ 1 TeV, in either channel, the windows are very wide and have only a lower threshold. For example for M_ℓ^* = 1 TeV the search windows are $\geq$744(720) GeV for electrons(muons). This is affordable as the background is of the order of 0.2 events.

At low masses, the narrow windows (driven by the simulated masses) do not overlap and between simulated mass points the windows are interpolated. The window parameters are optimized for the best expected exclusion limit. The signal selection efficiency is hardly affected by the L-shape selection. For $M_\ell^* >$1 TeV, where the search windows are sufficiently wide, no loss in signal selection efficiency is caused by this selection. As the search window width has to become more and more narrow with decreasing mass, this selection causes a reduction in signal efficiency by 10% for the lowest mass of M_ℓ^* = 250 GeV. This is outweighted by an improved signal-to-background ratio which increases the sensitivity to the second parameter of this analysis, the compositness scale Λ. The total signal selection efficiency for electrons(muons), including trigger, lepton and photon selection and Z-veto, has been determined to range between 24(28)% and 45(54)% for M_ℓ^* = 250 GeV and $\geq$2 TeV, respectively.

5.3 Systematic uncertainties

Two sources of uncertainties play a role, those which scale the yield without changing the shape and a second class affecting the shape of the invariant mass distributions. For each source of uncertainty summarized in Table 2, shifts of $\pm$1 standard deviation (σ) are applied, the kinematics of particles and objects (e, μ, γ) and resulting distributions ($M_{\ell\gamma}^{\min}$, $M_{\ell\gamma}^{\max}$) are recalculated, and the kinematic selection is reapplied. The difference with respect to the nominal situation is used to estimate the systematic uncertainty in the number of expected events. Several quantities, such as muon or electron resolution, are a function of p_T. This dependence is taken into account by applying the corresponding uncertainty event-by-event.

Systematic uncertainties on the signal selection include uncertainties on the lepton/photon ID, energy/momentum scale and resolution along with modeling of pileup events (5% uncertainty). The combined systematic uncertainty on signal selection is about 4%. Luminosity has been meassured with a precision of 2.7% [24] thus affecting the observed cross sections. For the signal cross sections k-factors account for higher-order corrections and 30% uncertainty on the k-factor is assumed. It is visible in the exclusion limits as a hatched band around the cross sections given for selected Λ values.

Specific uncertainties related to electrons, muons and photons are summarized in Table 2. The dominant impact in the muon channel for signal and simulated backgrounds derives from the uncertainty on pileup and the muon simulation-to-data scale factors (ID, isolation, etc). In the electron channel the dominant impact is from resolution and scale uncertainties which are correlated for electrons and photons.

Systematic uncertainties on simulated sample normalization and on backgrounds estimated from data are summarized in Section 4. Additionally, uncertainties on backgrounds estimated from simulation include the same uncertainties as applied to the leptons and photons in the

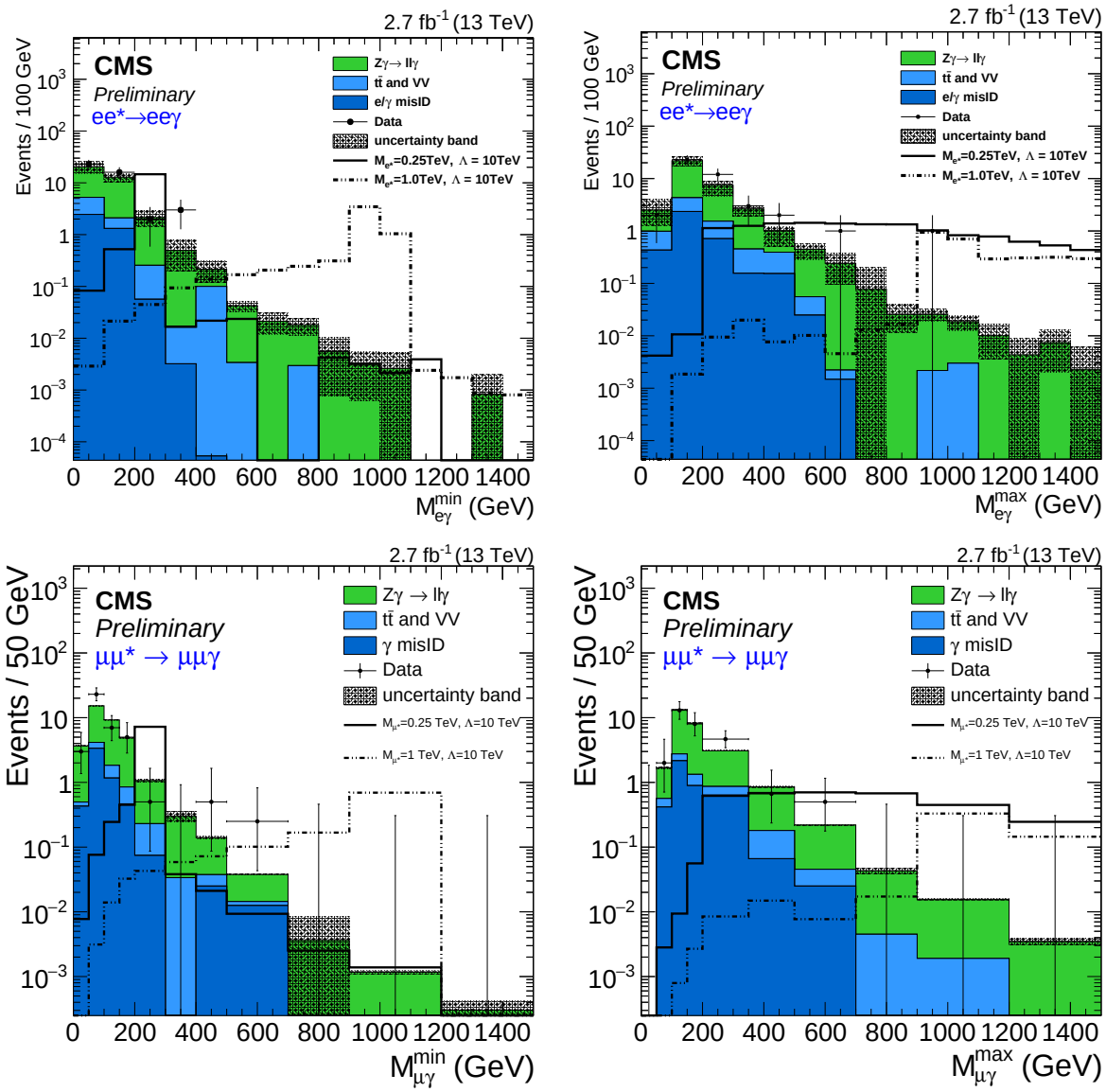

Figure 2: $M_{\ell\gamma}^{\min}$ and $M_{\ell\gamma}^{\max}$ for the electron channel in the upper row and the muon channel below. The different background contributions are shown in colors according to the legend. Also shown are two examples of potential ℓ^* signals.

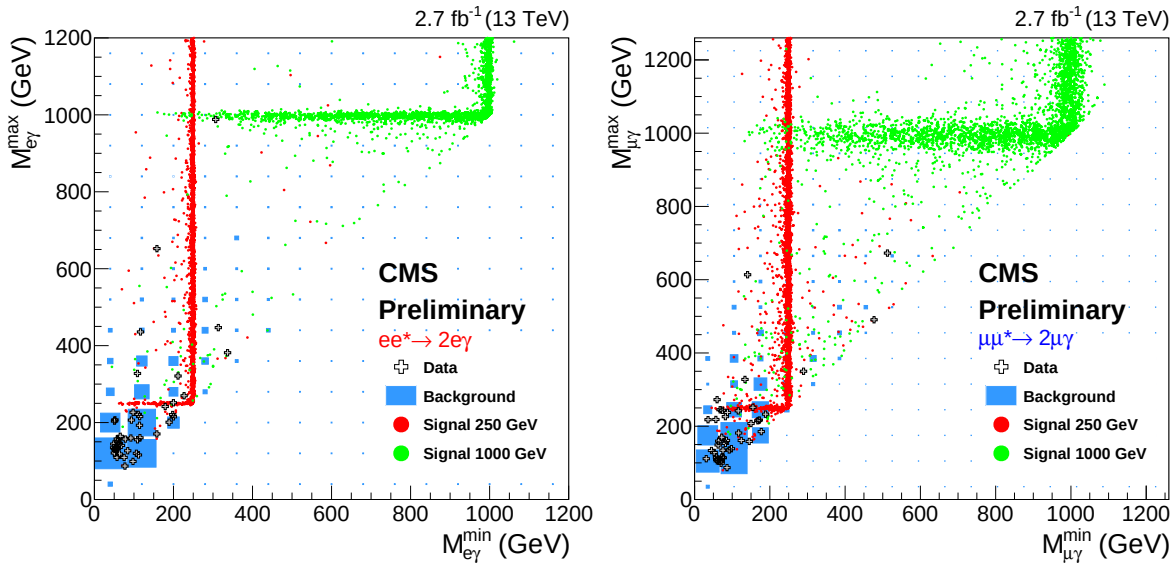

Figure 3: 2D $M_{\ell\gamma}^{\text{min}}$ versus $M_{\ell\gamma}^{\text{max}}$ distribution after full selection except the L-shaped search window, with expected background (blue), data (black crosses) and two signal examples for ℓ^* masses as given in the legend. The size of the blue squares for the background correspond to the number of events in a particular bin. On the left for the electron channel which has a high detector resolution over the full mass range. On the right for the muon channel where resolution degrades with mass. The background is weighted to the luminosity and the cross section.

signal samples and have similar impact to that in signal selections.

We use the PDF4LHC15 recommendations [36] to estimate the impact of various PDF sets. Therefore, we use the PDF4LHC15_30 sets that were obtained from the Hessian reduction method [37–39]. The impact on the background yield is very small and stays below 3%. The NNPDF3.0 set [40] was used for the simulation of the background. The impact on the signal acceptance times cross section is of the order of a few percent at low masses and at about 10% even at the highest excited lepton masses.

Table 2: Sources of systematic uncertainties. A range is provided for p_T -dependent uncertainties.

Uncertainty	Electrons	Muons
Luminosity	2.7%	2.7%
Pileup	5%	5%
$Z\gamma$ cross section	10%	10%
$Z\gamma$ high p_T k-factor	20%	20%
Photon fake ratio	10-40%	10-40%
Photon ID	1-2%	1-2%
Photon scale	4%	2%
Photon resolution	4%	2%
Electron fake rate	50%	–
Lepton ID	4% (barrel), 6% (endcap)	3%-8%
Lepton scale	4%	0.03(0.1)/TeV barrel(endcap)
Lepton resolution	4%	6(4)% at 1(0.3) TeV
Signal k-factor	30%	30%

6 Results

As no significant excess of data over the expected backgrounds is observed we set limits on the excited lepton parameters. The 95% confidence level (CL) upper limit on the excited lepton production cross section times branching fraction has been set using a single-bin counting method [41]. The computation has been performed using a Bayesian approach [42]. The resulting observed(expected) limits on the product of cross section and branching fraction are shown in Fig. 4 (left) as a solid(dashed) line, and with the one(two) standard deviation uncertainty bands labeled in green(yellow). They range from 0.25 fb to 10 fb as a function of M_ℓ^*. The black lines represent the theoretical cross sections including the NLO correction factors for given values of Λ. The theoretical cross section scales with Λ^{-4} while the shape of the $M_{\ell\gamma}^{\min}$, $M_{\ell\gamma}^{\max}$ distributions remains unchanged. The lower masses determine the limit on the compositness scale Λ which has to be above 15 TeV following this analysis. The limits on the compositness scale Λ are shown in Fig. 4 (right) and summarized in Tab.3. Limits on excited leptons are a function of the compositness scale, reaching 2.8(3.0) TeV for the electron(muon) channel for M_ℓ^* = Λ in this analysis. This improves the former exclusion limit of 2.5 TeV [11].

Table 3: Summary of the observed (expected) limits on ℓ^* mass, assuming $M_\ell^* = \Lambda$.

Search channel	$M_\ell^* = \Lambda$[TeV] observed (expected)	Best limit on Λ
eeγ	2.8 (2.9)	14(13) TeV
$\mu\mu\gamma$	3.0 (3.0)	15(15) TeV

The structure of the exclusion limits and of the related uncertainty bands is a consequence of the statistical variations from a small number of events varying between the tested M_ℓ^* points.

7 Summary

A search for excited leptons in the final state with two high p_T leptons and one photon has been performed using the 2015 data set of 2.7 fb^{-1} at $\sqrt{s}$=13 TeV recorded with the CMS detector. Events with a dilepton invariant mass significantly above the Z-pole mass, above 116 GeV, are selected. No significant excess is found and limits on the product of cross section and branching fraction are shown. Limits on the ℓ^* mass as a function of the compositness scale Λ exclude excited leptons below 2.8(3.0) TeV for the electron(muon) channel for $M_\ell^* = \Lambda$ and values of Λ up to more than 14(15) TeV at low M_ℓ^*.

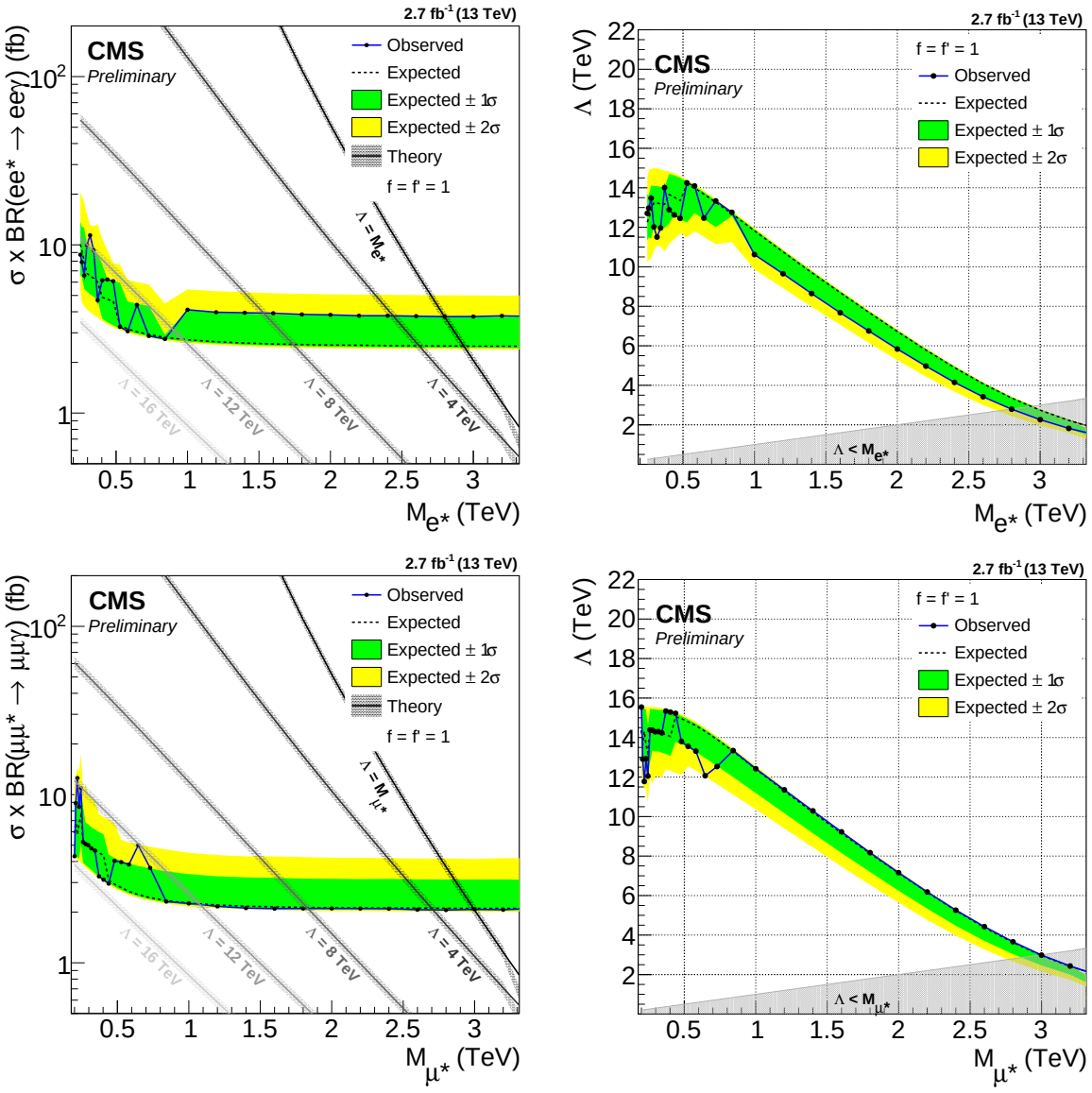

Figure 4: Exclusion limits for electrons (upper row) and muons (lower row). On the left the limit on the product of cross section and branching fraction. On the right the limit on the compositness scale Λ.

References

[1] J. C. Pati, A. Salam, and J. A. Strathdee, "Are quarks composite?", *Phys. Lett. B* **59** (1975) 265, doi:10.1016/0370-2693(75)90042-8.

[2] H. Terazawa, M. Yasuè, K. Akama, and M. Hayshi, "Observable effects of the possible substructure of leptons and quarks", *Phys. Lett. B* **112** (1982) 387, doi:10.1016/0370-2693(82)91075-9.

[3] M. Abolins et al., "Testing the Compositeness of Quarks and Leptons", in *Elementary Particles and Future Facilities (Snowmass 1982)*, p. 274. 1982. eConf C8206282.

[4] E. Eichten, K. D. Lane, and M. E. Peskin, "New Tests for Quark and Lepton Substructure", *Phys. Rev. Lett.* **50** (1983) 811, doi:10.1103/PhysRevLett.50.811.

[5] H. Harari, "Composite models for quarks and leptons", *Physics Reports* **104** (1984) 159, doi:10.1016/0370-1573(84)90207-2.

[6] K. D. Lane, F. E. Paige, T. Skwarnicki, and W. J. Womersley, "Simulations of supercollider physics", *Phys. Rept.* **278** (1997) 291, doi:10.1016/S0370-1573(96)00018-X, arXiv:hep-ph/9412280.

[7] U. Baur, M. Spira, and P. M. Zerwas, "Excited quark and lepton production at hadron colliders", *Phys. Rev. D* **42** (1990) 815, doi:10.1103/PhysRevD.42.815.

[8] O. W. Greenberg and C. A. Nelson, "Composite Models of Leptons", *Phys. Rev. D* **10** (1974) 2567, doi:10.1103/PhysRevD.10.2567.

[9] O. W. Greenberg and J. Sucher, "A quantum structure dynamic model of quarks, leptons, weak vector bosons, and Higgs mesons", *Phys. Lett. B* **99** (1981) 339, doi:10.1016/0370-2693(81)90113-1.

[10] CMS Collaboration, "Search for excited leptons in pp collisions at $\sqrt{s} = 7$ TeV", *Phys.Lett.* **B720** (2013) 309–329, doi:10.1016/j.physletb.2013.02.031, arXiv:1210.2422.

[11] CMS Collaboration, "Search for excited leptons in proton-proton collisions at sqrt(s) = 8 TeV", *JHEP* **03** (2016) 125, doi:10.1007/JHEP03(2016)125, arXiv:1511.01407.

[12] ATLAS Collaboration, "Search for excited leptons in proton-proton collisions at $\sqrt{s}$ = 7 TeV with the ATLAS detector", *Phys. Rev. D* **85** (2012) 072003, doi:10.1103/PhysRevD.85.072003, arXiv:1201.3293.

[13] ATLAS Collaboration, "Search for excited electrons and muons with 13 fb^{-1} of proton–proton collisions at $\sqrt{s} = 8$ TeV with the ATLAS detector", *ATLAS-CONF-2012-146* (Nov, 2012).

[14] ALEPH Collaboration, "Search for excited leptons at 130–140 GeV", *Phys. Lett. B* **385** (1996) 445, doi:10.1016/0370-2693(96)00961-6.

[15] DELPHI Collaboration, "Search for composite and exotic fermions at LEP 2", *Eur. Phys. J. C* **8** (1999) 41, doi:10.1007/s100529901074, arXiv:hep-ex/9811005.

[16] OPAL Collaboration, "Search for unstable heavy and excited leptons at LEP 2", *Eur. Phys. J. C* **14** (2000) 73, doi:10.1007/s100520050734, arXiv:hep-ex/0001056.

[17] L3 Collaboration, "Search for excited leptons at LEP", *Phys. Lett. B* **568** (2003) 23, doi:10.1016/j.physletb.2003.05.004, arXiv:hep-ex/0306016.

[18] H1 Collaboration, "Search for excited electrons in ep collisions at HERA", *Phys. Lett. B* **666** (2008) 131, doi:10.1016/j.physletb.2008.07.014, arXiv:0805.4530.

[19] CDF Collaboration, "Search for Excited and Exotic Electrons in the $e\gamma$ Decay Channel in $p\overline{p}$ Collisions at $\sqrt{s}$ = 1.96 TeV", *Phys. Rev. Lett.* **94** (2005) 101802, doi:10.1103/PhysRevLett.94.101802, arXiv:hep-ex/0410013.

[20] CDF Collaboration, "Search for Excited and Exotic Muons in the $\mu\gamma$ Decay Channel in $p\overline{p}$ Collisions at $\sqrt{s}$ = 1.96 TeV", *Phys. Rev. Lett.* **97** (2006) 191802, doi:10.1103/PhysRevLett.97.191802, arXiv:hep-ex/0606043.

[21] D0 Collaboration, "Search for excited muons in $p\overline{p}$ collisions at $\sqrt{s} = 1.96$ TeV", *Phys. Rev. D* **73** (2006) 111102, doi:10.1103/PhysRevD.73.111102, arXiv:hep-ex/0604040.

[22] D0 Collaboration, "Search for excited electrons in $p\overline{p}$ collisions at $\sqrt{s} = 1.96$ TeV", *Phys. Rev. D* **77** (2008) 091102, doi:10.1103/PhysRevD.77.091102, arXiv:0801.0877.

[23] CMS Collaboration, "The CMS experiment at the CERN LHC", *JINST* **03** (2008) S08004, doi:10.1088/1748-0221/3/08/S08004.

[24] CMS Collaboration, "CMS Luminosity Measurement for the 2015 Data Taking Period", *CMS Physics Analysis Summary CMS-PAS-LUM-15-001* (2015).

[25] T. Sjöstrand, S. Mrenna, and P. Z. Skands, "PYTHIA 6.4 physics and manual", *JHEP* **05** (2006) 026, doi:10.1088/1126-6708/2006/05/026, arXiv:hep-ph/0603175.

[26] T. Sjöstrand, S. Mrenna, and P. Z. Skands, "A brief introduction to PYTHIA 8.1", *Comput. Phys. Commun.* **178** (2008) 852, doi:10.1016/j.cpc.2008.01.036, arXiv:hep-ph/07103820.

[27] S. Majhi, "QCD corrections to excited lepton (pair) production at the LHC", *Phys. Rev. D* **88** (2013), no. 7, 074028, doi:10.1103/PhysRevD.88.074028, arXiv:1210.8307.

[28] J. Alwall et al., "The automated computation of tree-level and next-to-leading order differential cross sections, and their matching to parton shower simulations", *JHEP* **07** (2014) 079, doi:10.1007/JHEP07(2014)079, arXiv:1405.0301.

[29] P. Nason, "A New method for combining NLO QCD with shower Monte Carlo algorithms", *JHEP* **0411** (2004) 040, doi:10.1088/1126-6708/2004/11/040, arXiv:hep-ph/0409146.

[30] S. Frixione, P. Nason, and C. Oleari, "Matching NLO QCD computations with Parton Shower simulations: the POWHEG method", *JHEP* **0711** (2007) 070, doi:10.1088/1126-6708/2007/11/070, arXiv:0709.2092.

[31] S. Alioli, P. Nason, C. Oleari, and E. Re, "A general framework for implementing NLO calculations in shower Monte Carlo programs: the POWHEG BOX", *JHEP* **1006** (2010) 043, doi:10.1007/JHEP06(2010)043, arXiv:1002.2581.

[32] CMS Collaboration, "Performance of Electron Reconstruction and Selection with the CMS Detector in Proton-Proton Collisions at s = 8 TeV", *JINST* **10** (2015), no. 06, P06005, doi:10.1088/1748-0221/10/06/P06005, arXiv:1502.02701.

[33] CMS Collaboration, "Search for a Narrow Resonance Produced in 13 TeV pp Collisions Decaying to Electron Pair or Muon Pair Final States", *CMS Physics Analysis Summary CMS-PAS-EXO-15-005* (2015).

[34] CMS Collaboration, "Electron and Photon performance using data collected by CMS at $\sqrt{s}$ = 13 TeV and 25 ns", *CMS Detector Performance Summary CMS-DP-2015-067* (2015).

[35] CMS Collaboration, "Performance of Photon Reconstruction and Identification with the CMS Detector in Proton-Proton Collisions at sqrt(s) = 8 TeV", *JINST* **10** (2015), no. 08, P08010, doi:10.1088/1748-0221/10/08/P08010, arXiv:1502.02702.

[36] J. Butterworth et al., "PDF4LHC recommendations for LHC Run II", *J. Phys.* **G43** (2016) 023001, doi:10.1088/0954-3899/43/2/023001, arXiv:1510.03865.

[37] J. Gao and P. Nadolsky, "A meta-analysis of parton distribution functions", *JHEP* **07** (2014) 035, doi:10.1007/JHEP07(2014)035, arXiv:1401.0013.

[38] S. Carrazza et al., "An Unbiased Hessian Representation for Monte Carlo PDFs", *Eur. Phys. J.* **C75** (2015), no. 8, 369, doi:10.1140/epjc/s10052-015-3590-7, arXiv:1505.06736.

[39] G. Watt and R. S. Thorne, "Study of Monte Carlo approach to experimental uncertainty propagation with MSTW 2008 PDFs", *JHEP* **08** (2012) 052, doi:10.1007/JHEP08(2012)052, arXiv:1205.4024.

[40] NNPDF Collaboration, "Parton distributions for the LHC Run II", *JHEP* **04** (2015) 040, doi:10.1007/JHEP04(2015)040, arXiv:1410.8849.

[41] ATLAS and CMS Collaborations, "Procedure for the LHC Higgs boson search combination in Summer 2011", Technical Report CMS-NOTE-2011-005, ATL-PHYS-PUB-2011-011, CERN, Geneva, 2011.

[42] J. Heinrich et al., "interval estimation in the presence of nuisance parameters. 1. Bayesian approach", (2004). arXiv:physics/0409129.